Science Advances
AAAS

advances.sciencemag.org/cgi/content/full/6/16/eaaz9531/DC1

Supplementary Materials for

Molecular engineering of metal coordination interactions for strong, tough, and fast-recovery hydrogels

Wenxu Sun, Bin Xue, Qiyang Fan, Runhan Tao, Chunxi Wang, Xin Wang, Yiran Li, Meng Qin, Wei Wang*, Bin Chen*, Yi Cao*

*Corresponding author. Email: wangwei@nju.edu.cn (W.W.); chenb6@zju.edu.cn (B.C.); caoyi@nju.edu.cn (Y.C.)

Published 17 April 2020, *Sci. Adv.* **6**, eaaz9531 (2020)
DOI: 10.1126/sciadv.aaz9531

The PDF file includes:

Other Supplementary Material for this manuscript includes the following:

(available at advances.sciencemag.org/cgi/content/full/6/16/eaaz9531/DC1)

Materials and Methods

Materials

Histidine rich peptides and Aclt-HR-peptides were purchased from GL Biochem (Shanghai) Ltd. 4-Armed PEG-Aclt (Mw: 20000) was purchased from JenKem, Inc, China. Mal-PEG-NHS (MW: 5 kDa) was purchased from NanoCS. (3-mercaptopropyl) trimethoxysilane (MPTMS) was purchased from Sigma-Aldrich (shanghai, China). All other chemical reagents, unless otherwise stated, were purchased from Sinopharm Chemical Reagent Co., Ltd (China).

Scanning electron microscope (SEM)

SEM images were obtained using a Quanta Scanning Electron Microscope (Quata 200, FEI) at 20 kV. The hydrogels were dialyzed in Milli-Q water for 24 h to remove the unbound salts and lyophilized material prior to the measurement.

Swelling measurements

In a typical swelling experiment, the volume of the as-prepared HN-PH_n gels before dialysis was denoted as the initial volume (V_1), and the volume of the HN-PH_n gels after dialysis for 24 h in 1 M tris buffer (pH=7.60, containing 300 mM of KCl and an equal molar ratio of $ZnCl_2$ to the peptide binding sites) was denoted as the swollen volume (V_2). The swelling ratio ($\mathcal{E}$) was calculated as $\mathcal{E} = V_2/V_1$. All the experiments were undertaken at constant room temperature.

Loading rate dependent SMFS experiments

The AFM single molecule force spectroscopy measurements with five different pulling speeds (250 nm s^{-1}, 500 nm s^{-1}, 1000 nm s^{-1}, 2000 nm s^{-1}, 4000 nm s^{-1}) were performed. By fitting the data sets with Bell-Evans equation(*31*, *32*), the dissociation rates of binding (k_{off}) between different peptides and Zn^{2+} as well as the distance of the transition state or rupture distance (Δx) were quantified.

$$F = \frac{k_B T}{\Delta x} \ln\left(\frac{\Delta x}{k_{off} k_B T}\right) + \frac{k_B T}{\Delta x} \ln(r) \qquad (1)$$

F is the most probable rupture force, k_B is the Boltzmann constant, T is the absolute temperature.

SMFS experiments with EDTA as the competitive binding molecule

The SMFS experiments with EDTA as the competitive binding molecule were also carried out on a commercial AFM (JPK ForceRobot 300) at room temperature (~25 °C) as described in the Methods of the main text. In a typical experiment, EDTA was added into 1 M Tris buffer (pH=7.60, containing 300 mM KCl and 50 μM of $ZnCl_2$) to reach the final concentration of 1 mM after the normal force spectra was keeping achieved for more than half an hour. The sample rate of the data before and after the adding of EDTA was recorded.

UV spectroscopy measurements

Peptide and $ZnCl_2$ stock solutions were prepared in 1 M tris buffer (pH=7.60, containing 300 mM of KCl), respectively. Then the solutions were mixed in a 1:8 molar ratio to obtain a final peptide concentration of 0.5 mM and Zn^{2+} concentration of 4 mM. All the UV spectra was recorded using a V-550 (JASCO Inc., Japan) spectrophotometer. The cuvette width was 1 cm and the bandwidth was 0.2 nm. As shown in Fig. S1A-C, the

major UV absorption peak of the histidine imidazole ring was red-shifted by about 1 nm, 2 nm and 4 nm for PH_1, PH_3 and PH_6, respectively. The red-shift of the peak was due to the decrease of the electron density of the imidazole ring upon metal ion binding(*49*) . Moreover, the magnitude of the UV shift was consistent with the binding affinity of the peptides with Zn^{2+} ions measured by the ITC experiments.

Raman spectroscopy measurements

PH_1, PH_3 and PH_6 peptides were dissolved in ultrapure water to the concentration of 12, 4 and 2 mM, respectively. Next, desired amount of $ZnCl_2$ solution was added to achieve the final concentration of 12 mM. Then, the solution was adjusted to pH 8.0. 10 μL of each peptide solution was dried on a coverslip to form a peptide-metal ion film. These peptide-metal ion films were then analyzed on a confocal Raman microscope (alpha300, WITec) with a 532 nm laser under atmospheric conditions. The microscope was equipped with a piezo scanner (P-500, Physik Instrumente) and a 100x objective (Nikon, NA 0.6). The laser powers were lower than 2 mW during the measurements. The Raman scattered light was detected on a thermoelectrically cooled CCD detector (DU401A-BV, Andor) with an integration time of 10 s and 3 accumulations. For each sample, spectra from three randomly chosen positions were collected and averaged. The measurement and subsequent data analysis were performed with the software ScanCtrlSpectroscopyPlus (Version 1.38, WITec) and Project FOUR (Version 4.1 WITec). The peaks for $C_4{=}C_5$ vibrations of the imidazole ring were expected in the range from 1550–1640 cm^{-1}.(*50*) In the presence of Zn^{2+} ions, the histidine peaks in all the peptides shifted to 1601 cm^{-1}, indicating the coordination between histidine and Zn^{2+} ions (Fig. S1D-F)(*51*).

FT-IR spectroscopy measurements

The HN gels were prepared in a rectangular shape with thickness of about 1.5 mm. Then the IR spectra were recorded using a NICOLET iS10 (NICOLET, USA) spectrometer directly without drying the samples. The reported spectra were the average of more than 35 scans to increase the signal-to-noise ratio. The background signals were subtracted.

Using EDTA to reversibly tuning metal chelation of the peptides in hydrogels

The Zn^{2+} ions in HN-PH_n gels were removed by competitive binding by immersing the hydrogels in EDTA solutions (50 mM in 1 M Tris buffer containing 300 mM KCl, pH=7.60) for 48 h. To recharge the hydrogels with Zn^{2+} ions, the gels were first dialyzed in 1 M Tris buffer (pH=7.60, containing 300 mM KCl) for 48 h to remove the EDTA and then immersed 1 M Tris buffer (pH=7.60, containing 300 mM KCl and an equal molar ratio of $ZnCl_2$ to the peptide binding sites) to reform the coordination bonds.

Mesh size of the HN-PH_n gels

The HN-PH_n gels in the absence of Zn^{2+} ions were dialyzed in Milli-Q water for 24 h to remove the unbound salts and lyophilized prior to the measurement. Then the SEM images of the lyophilized samples were obtained using a Quanta Scanning Electron Microscope (Quata 200, FEI) at 20 kV. The meshes were marked with ImageJ and the size was measured according to the image scale.

Sol/gel fraction of the HN-PH_n gels without Zn^{2+} ions: The HN-PH_n gels without Zn^{2+} ions were dialyzed in 1 M Tris buffer (pH=7.60, containing 300 mM of KCl) for 24 hours and then in ddH_2O for another 24 hours to remove the salt. The hydrogel samples were weighted and the wet weight were recorded as W_1. Then the hydrogel samples were

lyophilized and the weight was recorded again as W_2. The sol/gel fraction (s) was calculated as $s = W_2/W_1 \times 100\%$.

Estimation of peptide concentrations in the HN-PH_n gels

The initial peptides added in the reaction mixtures to prepare the HN-PH_n gels were measured as (W_1). After the hydrogels were prepared, they were immersed into 8 × gel volume of 1 M Tris buffer (pH=7.60, containing 300 mM of KCl) and allowed to equilibrate for more than 24 hours. Then the mass of the peptides (W_2) not being incorporated in the hydrogel networks were estimated based on the UV absorbance at 220 nm of the released peptides in the buffer solution according to the calibration curves. The incorporated peptides were calculated as $\sigma = (W_1 - W_2)/W_1 \times 100\%$.

Calculation of the energetics of the free energy landscape

The calculation of the parameters describing the free energy landscape shown in *Table S1* was as follows: The free energy barrier of dissociation (ΔG_d) was calculated using the Arrhenius equation: $\Delta G_d = -RTln(\frac{A}{k_{off}})$, where R is the gas constant, T is the absolute temperature, k_{off} is the thermal off-rate at zero force achieved form the dynamic force spectroscopy measurements and A is the Arrhenius prefactor or the frequency factor. We chose A of 10^7 s^{-1} in our calculation. The energy barrier at the equilibrium state (ΔG_{eq}) can be calculated as follows: $\Delta G_{eq} = \Delta H - T\Delta S$, where ΔH is the enthalpy change and ΔS is the entropy change for the binding of HR-peptides with Zn^{2+} from the ITC measurements. The energy barrier of association (ΔG_a) was calculated as $\Delta G_a = \Delta G_d - \Delta G_{eq}$.

Multi-scale constitutive theory for hydrogels with metal-coordination interaction

Synthetic hydrogels, HN-PH_6, with metal ion binding complex PH_6 are firstly considered. As schematically shown in Fig. 6A, the synthetic material at the dry state without any formed peptide-Zn^{2+} is represented with a cube. Within this cube, eight chains cross-linked at the cubic center extend from the cubic center to each corner of the cube, as in the 8-chain model (*52*) . At the dry state, the cube of the represented volume element (RVE) is of dimension, $\bar{l}_0$. At the current state, the dimensions of RVE become l_1, l_2, and l_3, due to solvent absorption, metal ion binding, or mechanical loading, schematically shown in Fig. 6B. The volume of the RVE at the current state is assumed to be equal to the sum of the volume of a dry polymer network and that of the absorbed water (*53*), i.e.,

$$l_1 l_2 l_3 = \bar{l}_0^{\,3} + \Omega M, \qquad (2)$$

with Ω being the volume per water molecule and M the number of water molecules within the RVE.

Principal stretches of the RVE at the current state are given by $\lambda_1 = l_1/\bar{l}_0$, $\lambda_2 = l_2/\bar{l}_0$, and $\lambda_3 = l_3/\bar{l}_0$, respectively.

Dividing both sides of Eq. (2) by $\bar{l}_0^{\,3}$, we have

$$1 + \Omega C = \lambda_1 \lambda_2 \lambda_3, \qquad (3)$$

where $C = \frac{M}{\bar{l}_0^{\,3}}$ is the nominal concentration of water.

Three states are assigned for PH_6 within HN-PH_6, denoted as State "0", State "1", and State "2", respectively, illustrated in Fig. 3A. At State "0", PH_6-Zn^{2+} is not formed yet; At State "1", PH_6-Zn^{2+} is formed with only one binding site being associated; At State "2", PH_6-Zn^{2+} is formed with both binding sites being associated. Following the Bell-Evan's

model (*31*, *32*), the transition rate from State "1" to State "0", denoted as $K_{off}^{1\to0}$, is given by $K_{off}^{1\to0} = K_{off}^{0}\exp(\frac{\zeta_1 F}{F_b^{0ff}})$, (4)

Where F is the chain force, ζ_1 reflects the difference between the chain force and the force on PH_6-Zn^{2+} at State "1" and is set to be 2.0 in the analysis, K_{off}^{0} is the breaking rate at F=0, and F_b^{0ff} is a force scale. The transition rate from State "2" to State "1", denoted as $K_{off}^{2\to1}$, is given by $K_{off}^{2\to1} = 2K_{off}^{0}\exp\left(\frac{\zeta_2 F}{F_b^{0ff}}\right)$, with ζ_2 reflecting the difference between the chain force and the force on one binding site of PH_6-Zn^{2+} at State "2" and is set to be 1.0 in the analysis.

The transition rate from State "0" to State "1", denoted as $K_{on}^{0\to1}$, might be affected by a variety of factors, such as the elasticity of the binding pair, the elasticity of the local environment, initial length of the binding pair, separation of the binding pair depending on the deformation, the competition of neighboring available binding sites, etc. Here, a simple form for $K_{on}^{0\to1}$ is adopted, which is given by (*54*) $K_{on}^{0\to1} = K_{on}^{0}\exp\left(-\frac{\alpha_1\varepsilon}{k_BT}\right)$, where ε is the elastic energy within a PH_6-Zn^{2+} at State "1", K_{on}^{0} is the binding rate at ε=0, k_B is the Boltzmann constant, T is the temperature, and α_1 reflects the effect of the elasticity of the local environment. The transition rate from State "1" to State "2", is denoted as $K_{on}^{1\to2}$, given by (*54*) $K_{on}^{1\to2} = K_{on}^{1}\exp\left(-\frac{\alpha_2\varepsilon}{k_BT}\right)$, where K_{on}^{1} is the binding rate at ε=0 and α_2 reflects the effect of the elasticity of the local environment.

Let n_0, n_1, and n_2 be the average number of PH_6-Zn^{2+} existing between two neighboring covalently crosslinked sites within the chain network at State "0", at State "1", and at State "2", respectively. The effective total number of PH_6-Zn^{2+} existing between two neighboring covalently crosslinked sites within the chain network, denoted as n, is given by $n = n_0 + n_1 + n_2$.

It can then be derived that

$$\begin{aligned}\frac{dn_0}{dt} &= -K_{on}^{0\to1}n_0 + K_{off}^{0\leftarrow1}n_1\\ \frac{dn_1}{dt} &= K_{on}^{0\to1}n_0 - K_{off}^{0\leftarrow1}n_1 + K_{off}^{2\to1}n_2 - K_{on}^{1\to2}n_1,\\ \frac{dn_2}{dt} &= -K_{off}^{2\to1}n_2 + K_{on}^{1\to2}n_1\end{aligned} \quad (5)$$

The force-stretch curve of a polymer chain is described by the worm-like chain theory (*55*), given by

$F = \frac{k_BT}{\xi}[\frac{1}{4}\left(1-\frac{x}{L_c}\right)^{-2} - \frac{1}{4} + \frac{x}{L_c}]$, where ξ is the persistence length of the polymer chain and L_c is its contour length.

When PH_6-Zn^{2+} within the polymer network are dynamically formed or broken, L_c would change, given by $L_c = \frac{L_c^0}{n_1+n_2+1}$, where L_c^0 is the contour length of a polymer chain existing between two neighboring covalently crosslinked sites within the chain network.

In the theory, the current state of the RVE is defined by λ_1, λ_2, λ_3, n_0, n_1, and n_2 With n_0, n_1, and n_2 being fixed at the current state, the principle of virtual work is employed to solve the elastic field (*3*). Let the RVE at the current state change its dimensions by infinitesimal small amounts, δl_1, δl_2, and, δl_3. According to the principle of virtual work, the sum of the virtual work done by the applied forces, P_1, P_2, and P_3 and that by the chemical potential of water, μ, should be equal to the change in the internal energy within the RVE, denoted as δu, i.e.,

$$\delta u = P_1\delta l_1 + P_2\delta l_2 + P_3\delta l_3 + \mu\delta M. \quad (6)$$

With Eqs. (2, 6), we have

$$\delta u = \left(\sigma_1 + \frac{\mu}{\Omega}\right)\bar{l_0}^3\lambda_2\lambda_3\delta\lambda_1 + \left(\sigma_2 + \frac{\mu}{\Omega}\right)\bar{l_0}^3\lambda_3\lambda_1\delta\lambda_2 + \left(\sigma_3 + \frac{\mu}{\Omega}\right)\bar{l_0}^3\lambda_1\lambda_2\delta\lambda_3, \quad (7)$$

where σ_1, σ_2 and σ_3 are three principal true stresses, given by $\sigma_1 = \frac{P_1}{l_2 l_3}$, $\sigma_2 = \frac{P_2}{l_3 l_1}$ and $\sigma_3 = \frac{P_3}{l_1 l_2}$, respectively.

Due to fixed n_0, n_1 and n_2 at the current state, we also have

$$\delta u = \frac{\partial u}{\partial \lambda_1}\delta\lambda_1 + \frac{\partial u}{\partial \lambda_2}\delta\lambda_2 + \frac{\partial u}{\partial \lambda_3}\delta\lambda_3. \quad (8)$$

Combining Eq. (7) with Eq. (8) leads to

$$\left[\frac{\partial U}{\partial \lambda_1} - \left(\sigma_1 + \frac{\mu}{\Omega}\right)\lambda_2\lambda_3\right]\delta\lambda_1 + \left[\frac{\partial U}{\partial \lambda_2} - \left(\sigma_2 + \frac{\mu}{\Omega}\right)\lambda_3\lambda_1\right]\delta\lambda_2 + \left[\frac{\partial U}{\partial \lambda_3} - \left(\sigma_3 + \frac{\mu}{\Omega}\right)\lambda_1\lambda_2\right]\delta\lambda_3 = 0, \quad (9)$$

where $\delta U = \frac{\delta u}{\bar{l_0}^3}$.

Since $\delta\lambda_i$, i=1,2, and 3, in Eq. (9) are arbitrary and independent variables, it should be satisfied that

$$\begin{aligned}\sigma_1 &= \frac{1}{\lambda_2\lambda_3}\frac{\partial U}{\partial \lambda_1} - \frac{\mu}{\Omega}\\ \sigma_2 &= \frac{1}{\lambda_3\lambda_1}\frac{\partial U}{\partial \lambda_2} - \frac{\mu}{\Omega}\\ \sigma_3 &= \frac{1}{\lambda_1\lambda_2}\frac{\partial U}{\partial \lambda_3} - \frac{\mu}{\Omega}\end{aligned} \quad (10)$$

The change in U is the sum of the change in the elastic energy of polymer chains, and that in the energy of mixing water with polymers, i.e.,

$$\delta U = \delta U_1 + \delta U_2. \quad (11)$$

In Eq. (11), $\delta U_1 = \upsilon N\delta\varepsilon^{ch}$, where υ represents the portion of effective chains within the unit volume, N is the nominal density of polymer chains, given by $\mathrm{N} = 8/(\frac{2l_d}{\sqrt{3}})^3$, with l_d being the initial length of current polymer chains within the network, given by $\sqrt{2\xi L_c}$, and ε^{ch} is the elastic energy of a single polymer chain within the RVE at the current state, given by

$$\varepsilon^{ch} = \int_0^{(\lambda^{ch}-1)l_d} F dx = \frac{k_B T}{\xi}\left[\frac{1}{4}L_c\left(1 - \frac{(\lambda^{ch}-1)l_d}{L_c}\right)^{-1} - \frac{(\lambda^{ch}-1)l_d}{4} + \frac{(\lambda^{ch}-1)^2 {l_d}^2}{2L_c} - \frac{1}{4}L_c\right], \quad (12)$$

where λ^{ch} denotes the stretch of a polymer chain, given by $\lambda^{ch} = \sqrt{\frac{\lambda_1^2+\lambda_2^2+\lambda_3^2}{3}}$.

The energy of mixing water with polymers is given by (*53*)

$$U_2 = k_B T\left[C\log\frac{\Omega C}{1+\Omega C} + \frac{\chi C}{1+\Omega C}\right] \quad (13)$$

where χ is a measure of the interaction between polymer and water.

With Eqs. (12-13), we have

$$\begin{aligned}\sigma_1 &= \frac{\nu N\lambda_1^2}{\lambda_1\lambda_2\lambda_3}\frac{l_d F}{3\lambda} + \frac{k_B T}{\Omega}\left[\log\left(1 - \frac{1}{\lambda_1\lambda_2\lambda_3}\right) + \frac{1}{\lambda_1\lambda_2\lambda_3} + \frac{\chi}{\lambda_1^2\lambda_2^2\lambda_3^2}\right] - \frac{\mu}{\Omega}\\ \sigma_2 &= \frac{\nu N\lambda_2^2}{\lambda_1\lambda_2\lambda_3}\frac{l_d F}{3\lambda} + \frac{k_B T}{\Omega}\left[\log\left(1 - \frac{1}{\lambda_1\lambda_2\lambda_3}\right) + \frac{1}{\lambda_1\lambda_2\lambda_3} + \frac{\chi}{\lambda_1^2\lambda_2^2\lambda_3^2}\right] - \frac{\mu}{\Omega}\\ \sigma_3 &= \frac{\nu N\lambda_3^2}{\lambda_1\lambda_2\lambda_3}\frac{l_d F}{3\lambda} + \frac{k_B T}{\Omega}\left[\log\left(1 - \frac{1}{\lambda_1\lambda_2\lambda_3}\right) + \frac{1}{\lambda_1\lambda_2\lambda_3} + \frac{\chi}{\lambda_1^2\lambda_2^2\lambda_3^2}\right] - \frac{\mu}{\Omega}\end{aligned} \quad (14)$$

Following the procedure described above, constitutive equations for HN-PH_1 or HN-PH_3 can also be derived by noting that only two states are assigned for PH_1-Zn^{2+} in HN-PH_1 or PH_3-Zn^{2+} in HN-PH_3, as illustrated in Fig. 3A. In the subsequent analysis, the free swelling state is considered as the initial state with three principal true stresses being zero. The parameters employed in the analysis are listed in *Tables S3*. The theoretical predictions are displayed in Fig. 6C-F.

Figures

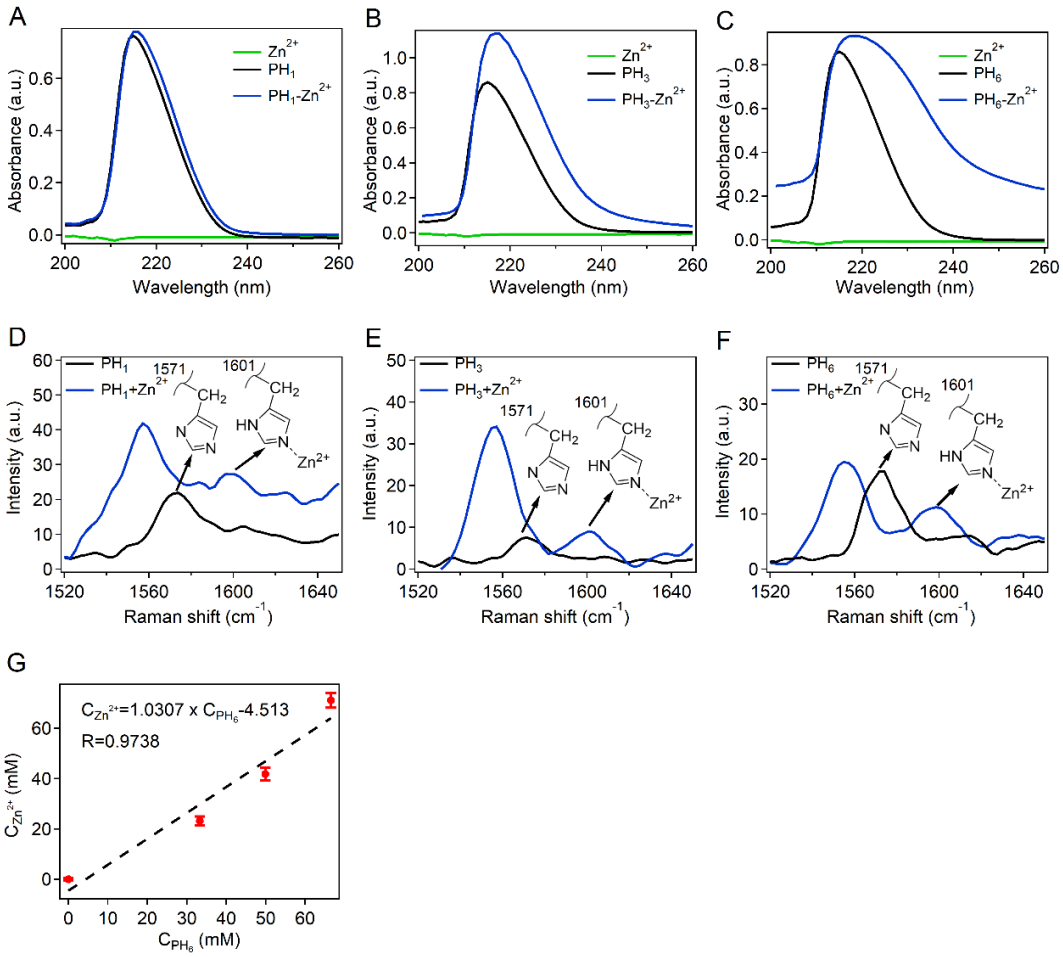

Fig. S1. Spectra characterization of HR peptides and molar ratios of zinc ions and the PH_6 peptide in HN-PH_6 gels. (A-C) UV spectra of PH_1 (A), PH_3 (B) and PH_6 (C) peptides (0.5 mM) without and with Zn^{2+} ions (4 mM) in 1 M Tris buffer (pH=7.60, containing 300 mM KCl). (D-F) Raman spectroscopy of PH_1 (D), PH_3 (E) and PH_6 (F) peptides formed at pH 7.6 without metals and with His: Zn^{2+} ratio of 1:1. The peptide-Zn^{2+} solutions were dried on top of glass slides beforex measurement. (G) The molar ratios of zinc ions and the PH_6 peptide in HN-PH_6 gels with different PH_6 concentrations. The red dots were calculated from X-ray fluorescence spectroscopy (XRFS) and the black dashed line was a linear fitting. The error bars correspond to the S.D. of three samples.

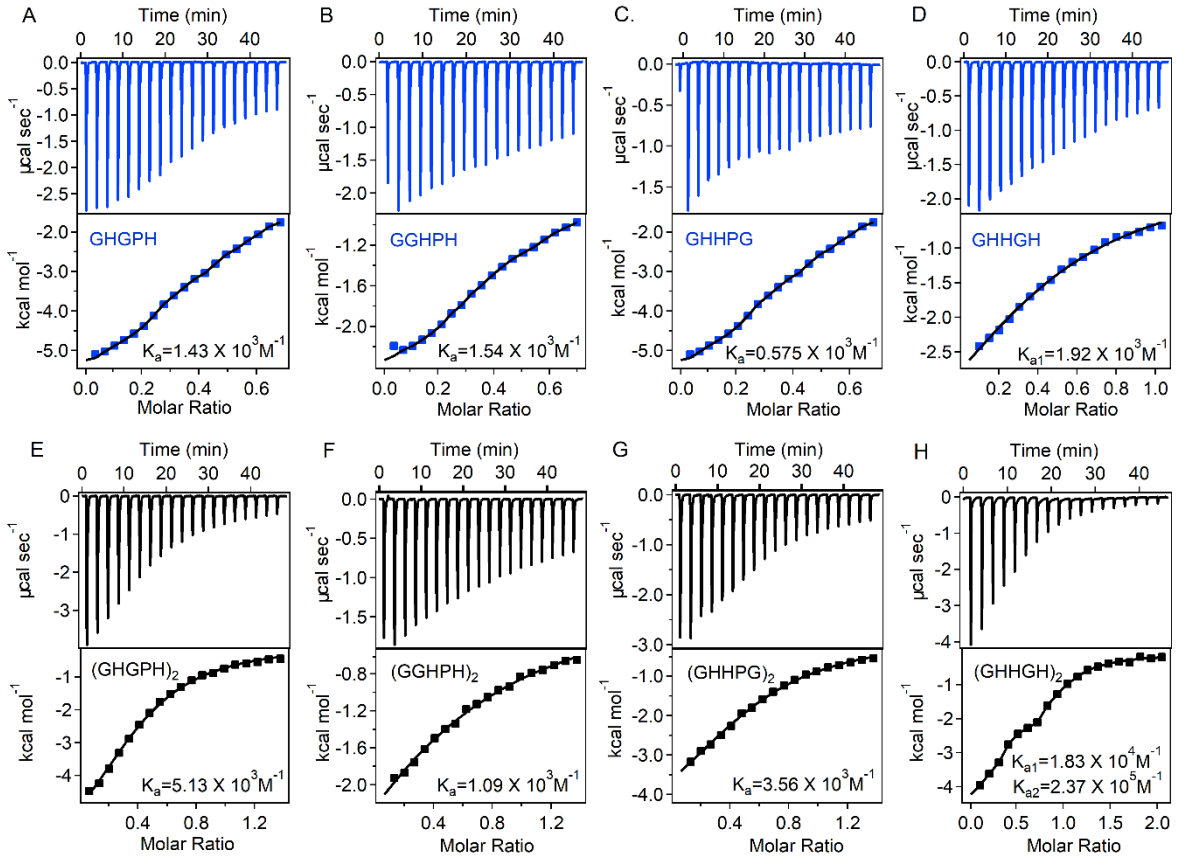

Fig. S2. The ITC titration data of different HR-peptides with $ZnCl_2$ in 1 M tris buffer (pH=7.60, containing 300 mM of KCl) at 25 °C to study the role of each amino-acid in the final peptide structure. (A-D) The ITC titration data of GHGPH, GGHPH, GHHPG and GHHGH peptides with $ZnCl_2$, respectively. (E-F) The ITC titration data of $(GHGPH)_2$, $(GGHPH)_2$, $(GHHPG)_2$ and $(GHHGH)_2$ peptides with $ZnCl_2$, respectively.

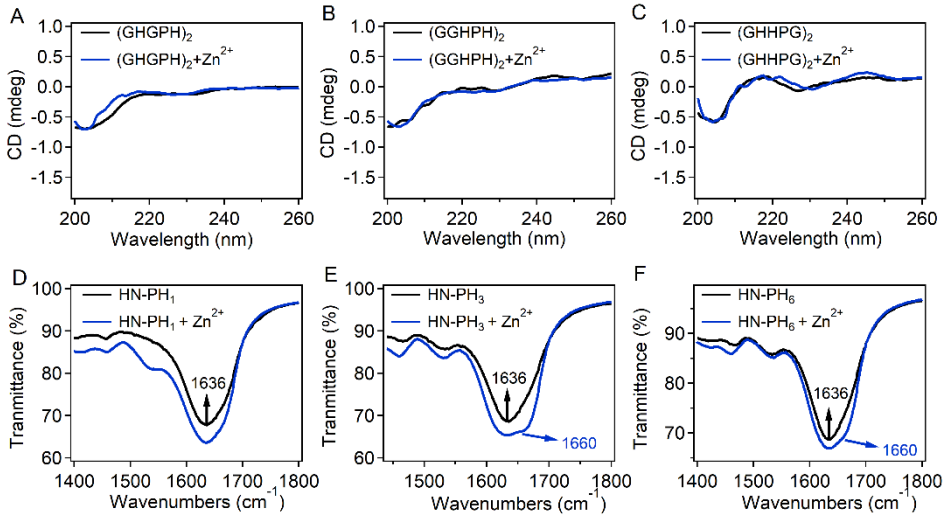

Fig. S3. Structure changes of HR peptides in the absence and presence of Zn^{2+} ions. (A-C) CD spectra of designed peptides in the absence and presence of Zn^{2+} ions. (A) $(GHGPH)_2$. (B) $(GGHPH)_2$. (C) $(GHHPG)_2$. (D-F) FT-IR spectroscopy of HN-PH_1 (D), HN-PH_3 (E) and HN-PH_6 (F) gels. In the absence of Zn^{2+} ions, all peptides adopted random coil structures with a major absorption peak at 1636 cm^{-1} in the absence of Zn^{2+} ions (*56*). Upon the addition of Zn^{2+} ions, a shoulder peak at 1660 cm^{-1} was observed for PH_3 and PH_6, suggesting the formation of PPII structure. Moreover, the shoulder peak of PH_6 was more obvious than that of PH_3, indicating that PH_6 was more structured when binding with Zn^{2+} ions than PH_3.

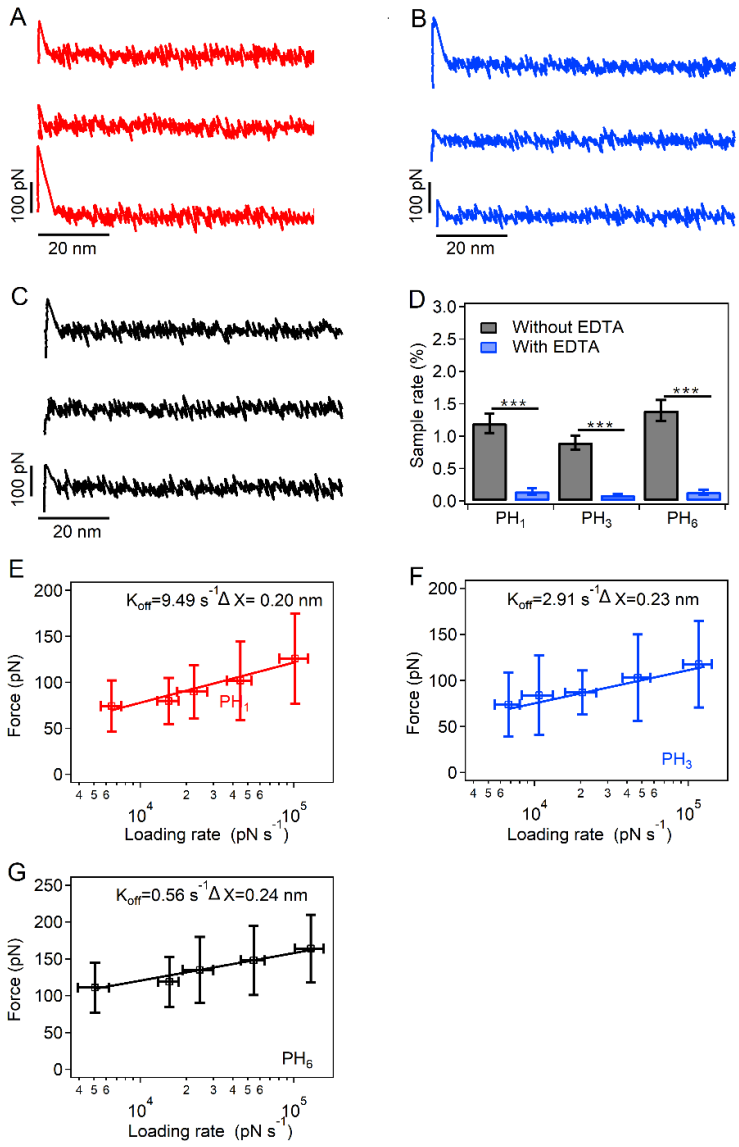

Fig. S4. Additional single-molecule force spectroscopy experiments. (A-C) Single-molecule force spectroscopy for the rupture of PH_n-Zn^{2+} complexes in the presence of EDTA. Typical force-extension curves for the rupture of PH_1-Zn^{2+} (red), PH_3-Zn^{2+}(blue), and PH_6-Zn^{2+} (black) complexes in 1 M Tris buffer with 1 mM EDTA, at a pulling speed of 1000 nm s^{-1}. In most traces, no rupture force peaks were observed. (D) The sample rate (the success rate to obtain force-extension curves showing the rupture of PH-Zn^{2+} complexes) of single-molecule force spectroscopy in 1M Tris buffer with and without 1 mM EDTA at a pulling speed of 1000 nm s^{-1}. (E) Loading-rate dependent rupture forces for PH_1-Zn^{2+} complexes. The red line corresponds to the fit by the Bell–Evans model. (F) Loading-rate dependent rupture forces for PH_3-Zn^{2+} complexes. The blue line corresponds to the fit by the Bell–Evans model. (G) Loading-rate dependent rupture forces for PH_6-Zn^{2+} complexes. The black line corresponds to the fit by the Bell–Evans model. Error bars indicate the mean ± S.D. ***: $p < 0.001$.

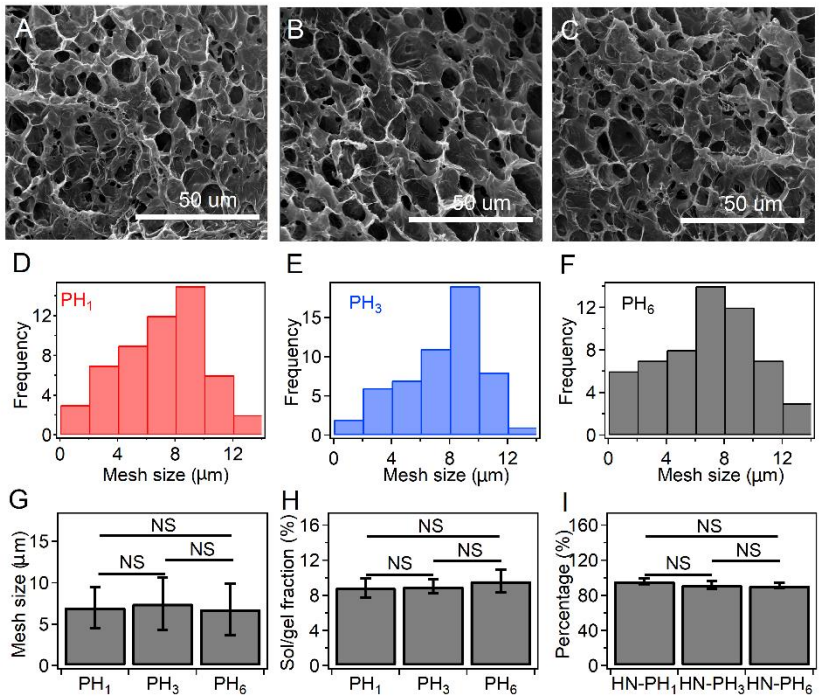

Fig. S5. Mesh size, sol/gel fractions, and the actual percent of peptides being incorporated to the hydrogel network. (A-C) SEM images of the HN-PH_1 gel (A), the HN-PH_3 gel (B) and the HN-PH_3 gel (C) before adding Zn^{2+} ions. (D-F) Mesh size distributions of the HN-PH_1 gel (D), HN-PH_3 gel (E) and HN-PH_6 gel (F) estimated from the SEM images using the ImageJ software. (G) Average mesh size of HN-PH_n gels in the absence of Zn^{2+} ions. (H) Sol/gel fractions of different HN-PH_n gels prior to adding zinc. (I) The percentage of peptides being incorporated in the hydrogel network. The initial peptide concentrations were 0.3 M, 0.10 M, and 0.05 M for PH_1, PH_3, and PH_6, respectively. The percentage of the peptides being incorporated in the hydrogels was similar, as estimated by subtracting the faction of eluted peptides from the total amount used. Error bars indicate the mean ± S.D. NS: $p > 0.05$.

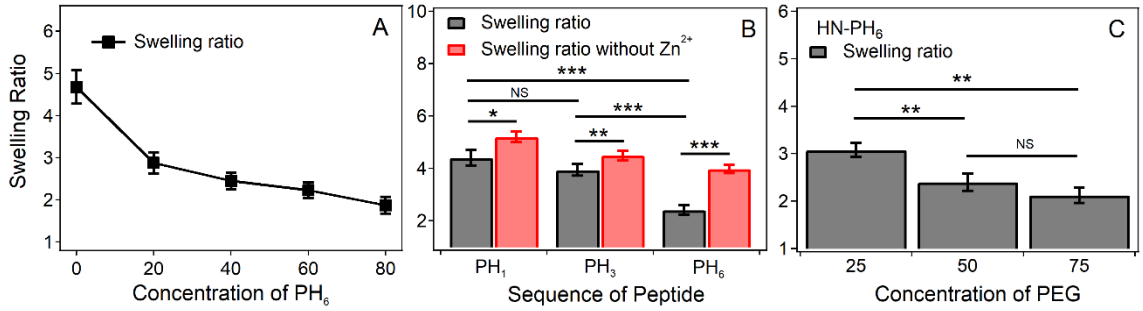

Fig. S6. Swelling behavior of the HN gels. (A) The swelling ratios of HN-PH_6 gels containing different concentrations (mg mL^{-1}) of PH_6 (B) The swelling ratios of HN-PH_n gels with or without zinc ions (molar concentrations of 0.05, 0.10, and 0.30 M for PH_6, PH_3, and PH_1, respectively). (C) The swelling ratios of HN-PH_6 gels containing different concentrations (mg mL^{-1}) of the primary cross-linker, 4-Armed PEG-Aclt. Error bars indicate the mean ± S.D, n=3. ***: $p < 0.001$.; **: $p < 0.01$; *: $p < 0.05$; NS: $p > 0.05$.

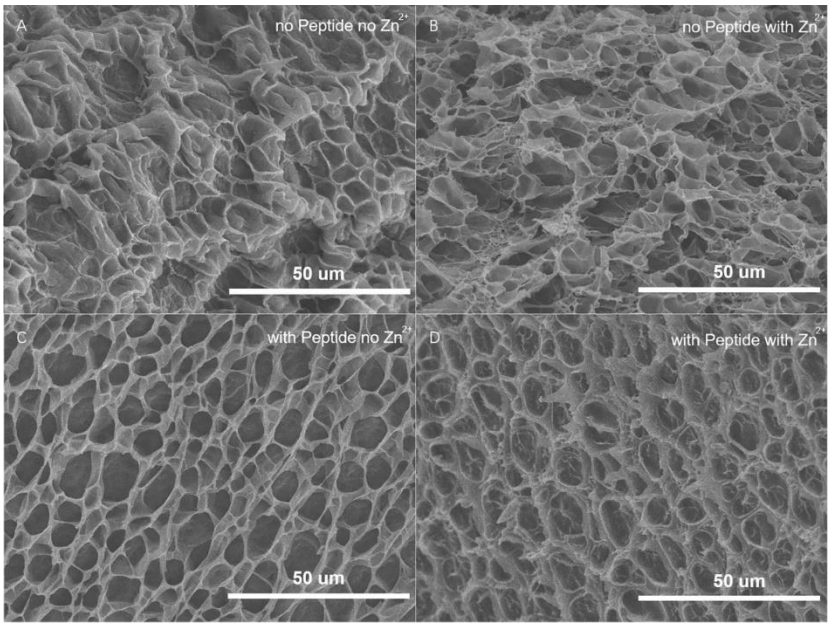

Fig. S7. SEM images of the HN-PH_6 gels. (A) Gel without PH_6 peptides and zinc ions. (B) Gel with zinc ions and without PH_6 peptides. (C) Gel with PH_6 peptides (0.05 M) but without zinc ions. (D) Gel containing both PH_6 peptides (0.05 M) and zinc ions.

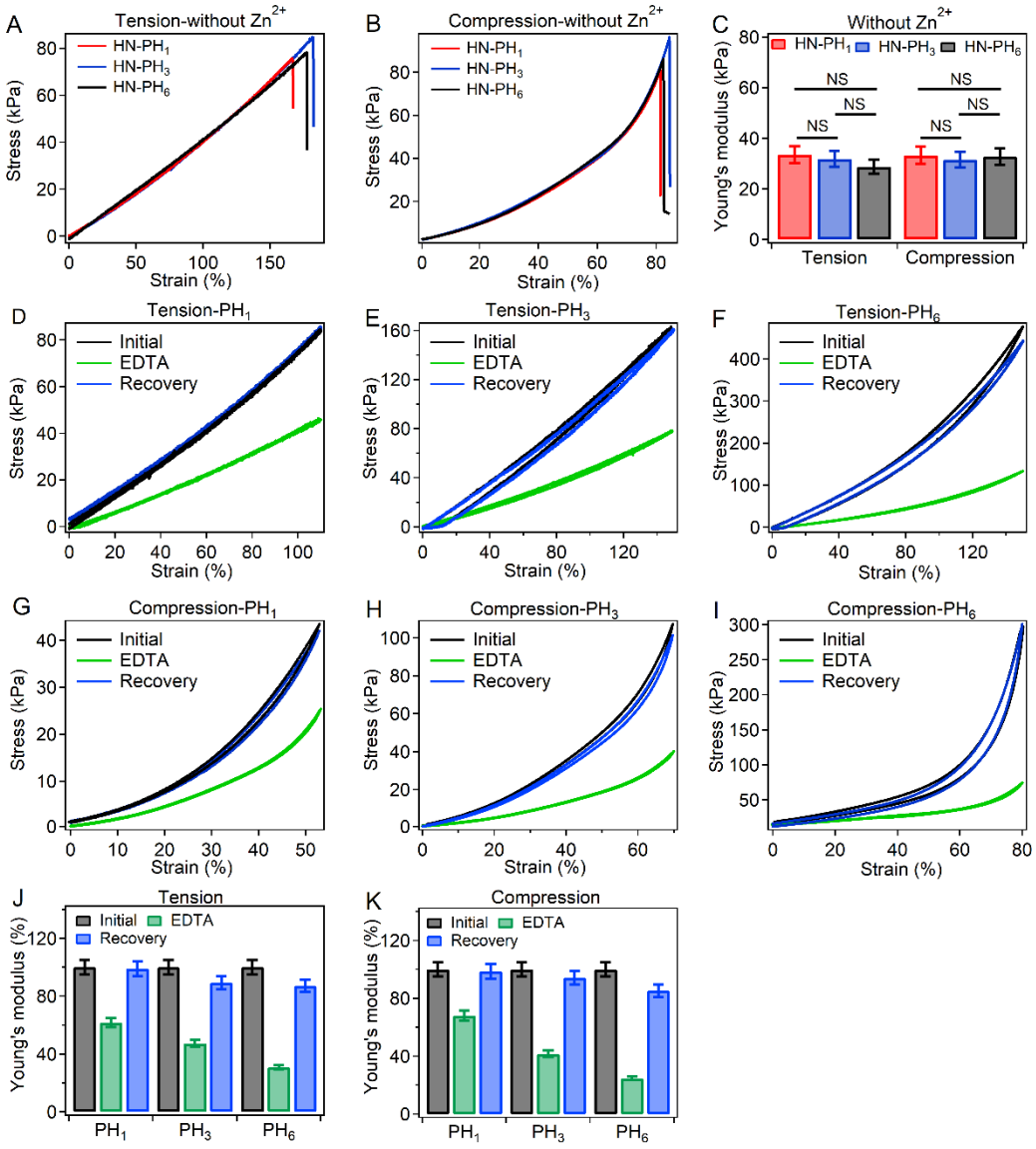

Fig. S8. Mechanical characterizations of the hydrogels without Zn^{2+} or perturbing the His-Zn interaction with EDTA. (A-B) Tensile (A) and compressive (B) stress-strain curves of the hydrogels without Zn^{2+}. (C) Young's modulus of HN-PH_1, HN-PH_3 and HN-PH_6 hydrogels without Zn^{2+}. Error bars indicate the mean ± S.D, n=3. NS: $p > 0.05$. (D-F) Tensile mechanical properties of initial HN-PH_n hydrogels, HN-PH_n hydrogels with EDTA and recovered HN-PH_n hydrogels recharging with Zn^{2+}. (G-I) Compressive mechanical properties of initial HN-PH_n hydrogels, HN-PH_n hydrogels with EDTA and recovered HN-PH_n hydrogels recharging with Zn^{2+}. (J) Normalized young's modulus of HN-PH_n hydrogels, HN-PH_n hydrogels with EDTA and recovered HN-PH_n hydrogels recharging with Zn^{2+} in tensile tests. Error bars indicate the mean ± S.D, n=3. (K) Normalized young's modulus of HN-PH_n hydrogels, HN-PH_n hydrogels with EDTA and recovered HN-PH_n hydrogels recharging with Zn^{2+} in compressive tests. Error bars indicate the mean ± S.D, n=3.

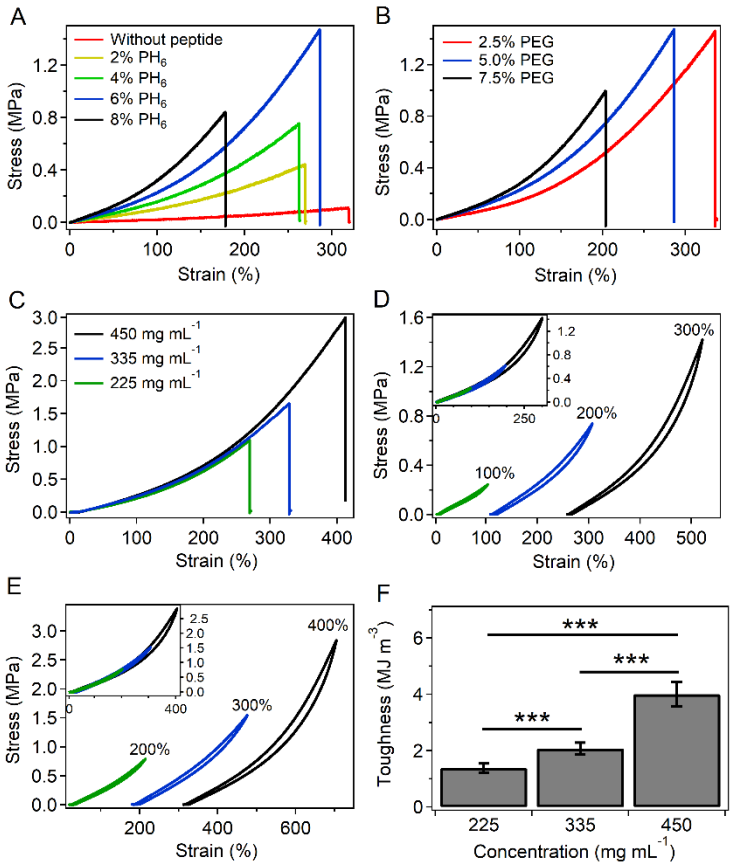

Fig. S9. Mechanical properties of the HN-PH_6 gels with varied PH_6, 4-Armed PEG-Aclt or acrylamide concentrations. (A) The uniaxial stretching stress-strain curve of HN-PH_6 gels at different PH_6 concentrations. (B) The uniaxial stretching stress-strain curve of HN-PH_6 gels at different 4-Armed PEG-Aclt concentrations. (C) Uniaxial stress-strain curves of HN-PH_6 gels with varied acrylamide concentrations under tension. (D) Uniaxial stretching-relaxation cycles of HN-PH_6 gels with acrylamide concentration of 335 mg mL^{-1} at different strains (100, 200 and 300%). The curves were offset for clarity and the overlapped curves are shown as the insets. (E) Uniaxial stretching-relaxation cycles of HN-PH_6 gels with acrylamide concentration of 450 mg mL^{-1} at different strains (200, 300 and 400%). The curves were offset for clarity and the overlapped curves are shown as the insets. (F) Toughness of HN-PH_6 gels with varied acrylamide concentrations. All the concentration reported here corresponded to the concentration before swelling. Error bars indicate the mean ± S.D of three samples. ***: $p < 0.001$.

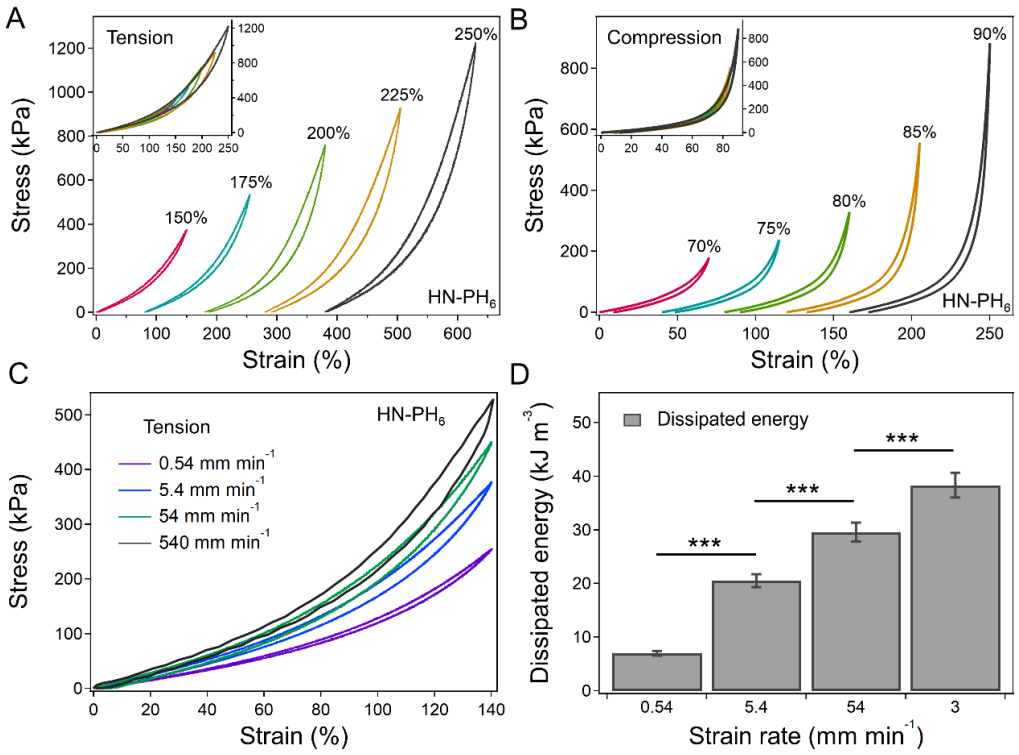

Fig. S10. Hysteresis of the HN-PH_6 hydrogels at different strains and strain rates. (A) and (B) Uniaxial stretching/compression-relaxation cycles of HN-PH_6 gels at different strains. The curves were offset for clarity and the overlapped curves are shown as the insets. (C) Uniaxial stretching-relaxation cycles of HN-PH_6 hydrogels at the strain rates of 0.54, 5.4, 54 and 540 mm min^{-1}. (D) Summarized dissipated energy of HN-PH_6 hydrogels at the strain rates of 0.54, 5.4, 54 and 540 mm min^{-1}. Error bars indicate the mean ± S.D of three samples. ***: $p < 0.001$.

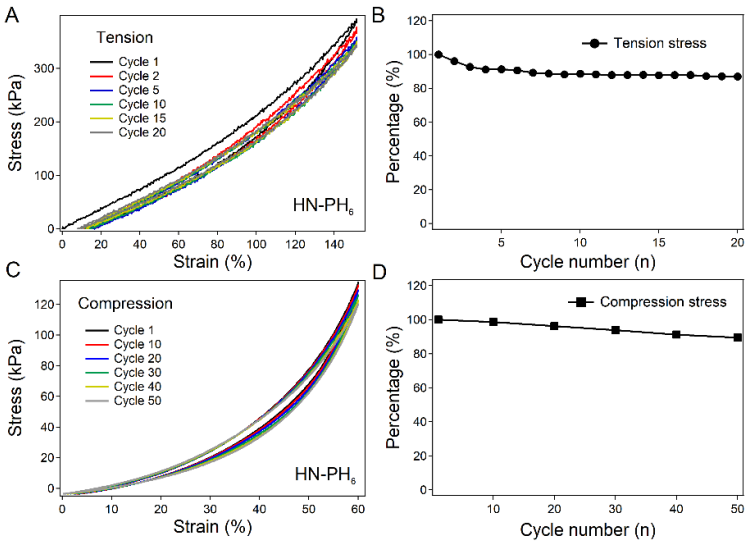

Fig. S11. Mechanical performance of HN-PH_6 gels in the multi-cycle tests without any waiting time. (A) Stretching-relaxation cycles of the same HN-PH_6 gel for 20 consecutive cycles without waiting between each cycle. (B) The maximum tensile stress of the HN-PH_6 gel in the 20 cycles shown in (A). (C) The compression-relaxation cycles of the same

HN-PH_6 gel for 50 consecutive cycles without waiting between each cycle. (D) The maximum compressive stress of the HN-PH_6 gel in the 50 cycles shown in (C).

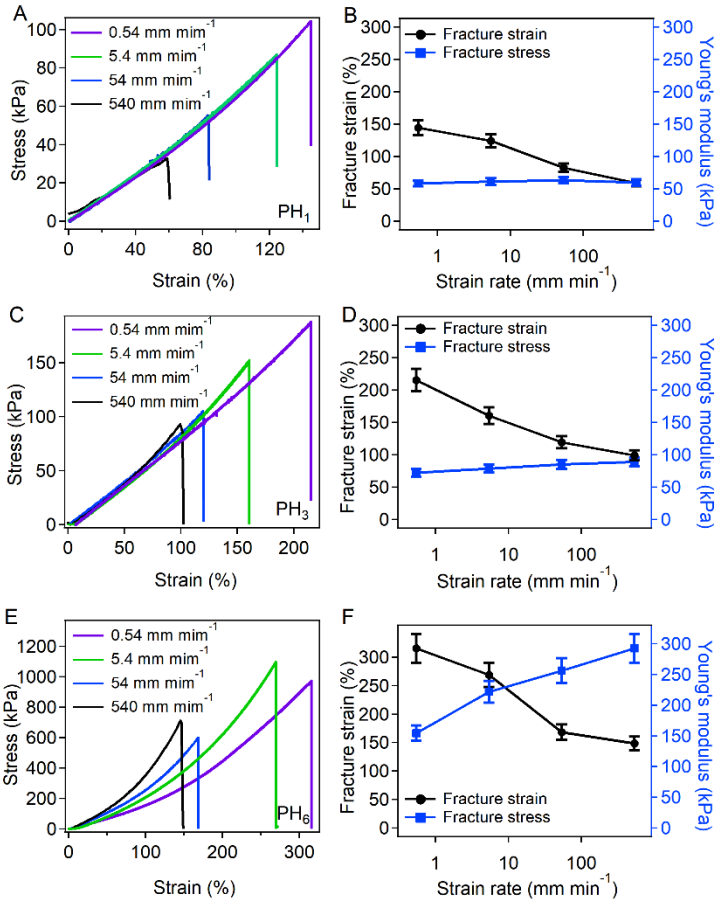

Fig. S12. Tensile mechanical properties of the HN-PH_n hydrogels at different strain rates. (A) Uniaxial stress-strain curves of HN-PH_1 hydrogels under tension at the strain rates of 0.54, 5.4, 54 and 540 mm min^{-1}. (B) Summarized fracture strain and Young's modulus of HN-PH_1 hydrogels at the strain rates of 0.54, 5.4, 54 and 540 mm min^{-1}. (C) Uniaxial stress-strain curves of HN-PH_3 hydrogels under tension at the strain rates of 0.54, 5.4, 54 and 540 mm min^{-1}. (D) Summarized fracture strain and Young's modulus of HN-PH_3 hydrogels at the strain rates of 0.54, 5.4, 54 and 540 mm min^{-1}. (E) Uniaxial stress-strain curves of HN-PH_6 hydrogels under tension at the strain rates of 0.54, 5.4, 54 and 540 mm min^{-1}. (F) Summarized fracture strain and Young's modulus of HN-PH_6 hydrogels at the strain rates of 0.54, 5.4, 54 and 540 mm min^{-1}. Error bars indicate the mean ± S.D of three samples.

Table S1. Free energy landscape for the binding/unbinding of Zn^{2+} with PH_1, PH_3 and PH_6 peptides. Data are presented as average ± s.d. *

	K_{off} (s^{-1})	ΔH (kJ mol^{-1})	ΔS (kJ mol^{-1} deg^{-1})	ΔG_a (kJ mol^{-1})	ΔG_{eq} (kJ mol^{-1})	ΔG_d (kJ mol^{-1})
PH_1	9.49 ±5.34	-16.14 ±1.35	-0.056 ± 0.0047	-29.75 ± 0.41	-4.62 ± 2.3	-34.36 ± 1.57
PH_3	2.91 ±1.28	-32.99 ± 2.73	-0.069 ± 0.0021	-24.87 ± 0.93	-12.43 ± 0.68	-37.30 ± 1.18
PH_6	0.56 ±0.45	-17.20 ± 0.96 (ΔH_1) -15.45 ± 0.66 (ΔH_2)	-0.076 ± 0.0031 (ΔS_1) -0.033 ± 0.0013 (ΔS_2)	-30.3 ± 2.11	-5.45 ± 0.94 (ΔG_{eq1}) -5.62 ± 0.52 (ΔG_{eq2})	-41.37 ± 2.75

* There are two ΔH and ΔS values from the ITC measurements of PH_6 and Zn^{2+} binding since PH_6 has two binding sites.

Table S2. Mechanical properties of PAM, HN-PH_1, HN-PH_3 and HN-PH_6 gels containing different concentrations of peptides. Data are presented as average ± s.d. *

	Molar concentration of HR-peptide (mM)	Swelling ratio (V/V)	Tension strain limit (%)	Tension stress limit (kPa)
PAM	/	4.68 ± 0.41	282.08 ± 33.04	106.05 ± 2.93
HN-PH_1	300	4.41 ± 0.30	125.29 ± 15.80	83.35 ± 20.15
HN-PH_3	100	3.93 ± 0.22	179.05 ± 13.49	169.67 ± 15.19
HN-PH_6	16.7	2.88 ± 0.25	243.91 ± 17.89	413.36 ± 23.32
	33.3	2.45 ± 0.20	246.16 ± 15.43	715.38 ± 30.17
	50	2.23 ± 0.18	275.45 ± 7.31	1379.08 ± 166.09
	66.6	1.87 ± 0.20	172.94 ± 18.47	807.00 ± 70.96
	Compression strain limit (%)	**Compression stress limit (kPa)**	**Young's modulus (kPa)**	**Toughness (kJ m^{-3})**
PAM	85.59 ± 2.78	75.24 ± 6.10	26.95 ± 6.73	143.76 ± 17.79
HN-PH_1	71.45 ± 2.09	46.88 ± 3.38	58.61 ± 4.97	50.27 ± 17.51
HN-PH_3	86.47 ± 2.24	128.20 ± 7.66	70.52 ± 6.47	136.83 ± 15.13
HN-PH_6	89.81 ± 1.77	224.43 ± 12.99	100.78 ± 10.36	420.94 ± 36.35
	84.78 ± 2.14	343.74 ± 15.56	150.43 ± 4.39	683.15 ± 49.94
	94.10 ± 1.49	1005.67 ± 74.77	221.37 ± 7.72	1327.76 ± 125.67
	72.58 ± 1.82	350.43 ± 24.29	303.53 ± 5.56	571.83 ± 94.59

* PAM gel refers to hydrogels containing only the primary network: polyacrylamide cross-linked by 4-Armed PEG-Aclt. All hydrogels were charged by Zn^{2+} ions.

Table S3. Parameters for simulation of uniaxial stretching (S)/compression (C)- relaxation of gels

Default parameters		L_c^0 (nm)	80 nm		Ω (nm^3)	0.03 (53)
		k_BT (pN•nm)	4.14		μ	0
		χ	0.2 (53)		ζ_1	2
		$\bar{l}_0$(nm)	9.24		ζ_2	1
		v	0.6			
		Loading rate for uniaxial stretch-relaxation (/min)				0.3
		Loading rate for uniaxial compression-relaxation (/min)				0.1
Parameters of different gels		DN-PH_1	DN-PH_3	DN-PH_6	DN-PH_{3R1}	DN-PH_{3R2}
k_{on}^0 (s^{-1})	S	3.96×10^2	6.31×10^2	7.81×10^2	7.81×10^2	2.65×10^5
	C	3.96×10^2	6.31×10^2	7.81×10^2	7.81×10^2	2.65×10^5
k_{on}^1 (s^{-1})	S	—	—	2.65×10^5	—	—
	C	—	—	2.65×10^5	—	—
α_1	S	0.3	0.4	0.4	0.4	0.01
	C	0.5	0.4	0.4	0.4	0.14
α_2	S	—	—	0.01	—	—
	C	—	—	0.32	—	—
k_{off}^0 (s^{-1})	S	9.49	2	0.56	0.56	0.56
	C	9.49	2	0.56	0.56	0.56

F_b^{off} (pN)	S	20.61	17.92	17.18	17.18	17.18
	C	20.61	17.92	17.18	17.18	17.18
n	S	20	8	3	3	3
	C	20	8	3	3	3
Parameters of gels with different content of PH6		DN-PH_6 (0%)	DN-PH_6 (2%)	DN-PH_6 (4%)	DN-PH_6 (6%)	DN-PH_6 (8%)
k_{on}^0 (s^{-1})	S	7.81×10^2	7.81×10^2	7.81×10^2	7.81×10^2	7.81×10^2
	C	7.81×10^2	7.81×10^2	7.81×10^2	7.81×10^2	
k_{on}^1 (s^{-1})	S	2.65×10^5	2.65×10^5	2.65×10^5	2.65×10^5	2.65×10^5
	C	2.65×10^5	2.65×10^5	2.65×10^5	2.65×10^5	
α_1	S	0.4	0.4	0.4	0.4	0.4
	C	0.4	0.4	0.4	0.4	
α_2	S	0.01	0.01	0.01	0.01	0.01
	C	0.32	0.32	0.32	0.32	
k_{off}^0 (s^{-1})	S	0.56	0.56	0.56	0.56	0.56
	C	0.56	0.56	0.56	0.56	
F_b^{off} (pN)	S	17.18	17.18	17.18	17.18	17.18
	C	17.18	17.18	17.18	17.18	
n	S	0	1	2	3	4
	C	0	1	2	3	

Table S4. Mechanical properties of HN-PH_6 gels and other tough hydrogels.

Sample code	Water content (wt%)	Young's modulus (MPa)	Break strain (mm/mm)	Fracture strength (MPa)	Toughness (MJ m^{-3})	Fracture energy (kJ m^{-2})	Recovery time (min)	Recovery efficiency (%)
HN-PH_6*	80.4	0.27	4.12	3.02	4.03	--	0	~85
St(PGs)-DN3(*2*)	87	0.33	4.73	0.96	3.7	--	--	--
St(HA)-DN1(*2*)	89.4	0.1	1.97	1.15	1.16	--	--	--
St(CS)-DN4(*2*)	88.43	0.3	4.26	0.71	2.26	--	--	--
Supramolecular polymer network(*8*)	80	0.016-0.42	107	1.8	--	--	30	~100
L-NC gel(*9*)	62	43.2	7.4	1.6	7.38	--	--	--
B-DN3 gel(*11*)	44 ± 2	22 ± 0.2	5.7 ± 0.7	10.5 ± 1.4	--	2.85 ± 0.22	5	~85
CCP-MCP1 gel(*12*)	32	0.145	5.49	2.6	--	1.33	>15	--
Hybrid gel(*13*)	86	0.029	23	0.156	--	8.7	1440	74
DN-Sul gel(*14*)	54.6	0.8	5.05	3.7	7.6	9.8	240	>90
DN-Cit gel(*14*)	56.9	1.3	5	5.6	12.1	14	240	96.6
P(urea-IL_a-$SPMA_b$)-3d gel(*15*)	~50	1.97 ± 0.12	4.78 ± 0.24	1.90 ± 0.12	6.70 ± 0.10	--	120	~85
Agar/PAM gel(*16*)	79.4	0.082	22.4	1.23	8.96	--	10 (100 ^oC)	~90
EG-15 gel(*17*)	~65	~12.5	~4.7	~12	~40	--	240	78
D-hydrogel-0.15(*18*)	60-70	~1.75	7.48	5.9	27.2 ± 1.01	--	240	87.6
PAM-CS-A DN gel(*19*)	~80	0.318 ± 0.042	4.7	2.12	--	12.9 ± 1.3	240	95
PAM-CS-S DN gel(*19*)	~80	0.357 ± 0.045	5.6	1.94	--	8.3 ± 0.8	240	90
Crystallized PVA-PAAm gel(*20*)	62	5	~3.8	2.5	--	14	1440	>90
$(FL)_8$ gel(*23*)	70	0.016 ± 0.003	4.5 ± 0.9	0.035 ± 0.006	--	--	20	~85
CB[8] gel(*35*)	90	0.0046	24	~130	--	0.75 ± 0.04	3	~100
PU/DHIR-0.244-20% gel(*57*)	82.35 ± 0.26	2.14 ± 0.43	8.25 ±0.59	4.79 ± 0.55	--	2.493 ± 0.138	360	~100

Movie S1: Cyclic compression of the HN-PH_6 hydrogel (to ~70% strain) at a frequency of ~1.6 Hz.

Movie S2: Cyclic stretching of the HN-PH_6 hydrogel (to ~150% stain) at a frequency of ~1.6 Hz.

Movie S3: Compressing the HN-PH_6 hydrogel using a sharp blade.

REFERENCES AND NOTES

1. H. Yuk, S. Lin, C. Ma, M. Takaffoli, N. X. Fang, X. Zhao, Hydraulic hydrogel actuators and robots optically and sonically camouflaged in water. *Nat. Commun.* **8**, 14230 (2017).

2. Y. Zhao, T. Nakajima, J. J. Yang, T. Kurokawa, J. Liu, J. Lu, S. Mizumoto, K. Sugahara, N. Kitamura, K. Yasuda, A. U. D. Daniels, J. P. Gong, Proteoglycans and glycosaminoglycans improve toughness of biocompatible double network hydrogels. *Adv. Mater.* **26**, 436–442 (2014).

3. J. Wu, P. Li, C. Dong, H. Jiang, X. Bin, X. Gao, M. Qin, W. Wang, C. Bin, Y. Cao, Rationally designed synthetic protein hydrogels with predictable mechanical properties. *Nat. Commun.* **9**, 620 (2018).

4. J.-Y. Sun, C. Keplinger, G. M. Whitesides, Z. Suo, Ionic skin. *Adv. Mater.* **26**, 7608–7614 (2014).

5. C. Cvetkovic, R. Raman, V. Chan, B. J. Williams, M. Tolish, P. Bajaj, M. S. Sakar, H. H. Asada, M. T. A. Saif, R. Bashir, Three-dimensionally printed biological machines powered by skeletal muscle. *P. Natl. Acad. Sci. U.S.A.* **111**, 10125–10130 (2014).

6. C. Creton, 50th anniversary perspective: Networks and gels: Soft but dynamic and tough. *Macromolecules* **50**, 8297–8316 (2017).

7. J. P. Gong, Y. Katsuyama, T. Kurokawa, Y. Osada, Double-network hydrogels with extremely high mechanical strength. *Adv. Mater.* **15**, 1155–1158 (2003).

8. J. Liu, C. S. Y. Tan, Z. Yu, N. Li, C. Abell, O. A. Scherman, Tough supramolecular polymer networks with extreme stretchability and fast room-temperature self-healing. *Adv. Mater.* **29**, 1605325 (2017).

9. J. Wang, L. Lin, Q. Cheng, L. Jiang, A strong bio-inspired layered PNIPAM–Clay nanocomposite hydrogel. *Angew. Chem. Int. Ed. Engl.* **51**, 4676–4680 (2012).

10. Y. Okumura, K. Ito, The polyrotaxane gel: A topological gel by figure-of-eight cross-links. *Adv. Mater.* **13**, 485–487 (2001).

11. H. J. Zhang, T. L. Sun, A. K. Zhang, Y. Ikura, T. Nakajima, T. Nonoyama, T. Kurokawa, O. Ito, H. Ishitobi, J. P. Gong, Tough physical double-network hydrogels based on amphiphilic triblock copolymers. *Adv. Mater.* **28**, 4884–4890 (2016).

12. M. A. Gonzalez, J. R. Simon, A. Ghoorchian, Z. Scholl, S. Lin, M. Rubinstein, P. Marszalek, A. Chilkoti, G. P. López, X. Zhao, Strong, tough, stretchable, and self-adhesive hydrogels from intrinsically unstructured proteins. *Adv. Mater.* **29**, 1604743 (2017).

13. J.-Y. Sun, X. Zhao, W. R. K. Illeperuma, O. Chaudhuri, K. H. Oh, D. J. Mooney, J. J. Vlassak, Z. Suo, Highly stretchable and tough hydrogels. *Nature* **489**, 133–136 (2012).

14. Y. Yang, X. Wang, F. Yang, L. Wang, D. Wu, Highly elastic and ultratough hybrid ionic–Covalent hydrogels with tunable structures and mechanics. *Adv. Mater.* **30**, e1707071 (2018).

15. T. Long, Y. Li, X. Fang, J. Sun, Salt-mediated polyampholyte hydrogels with high mechanical strength, excellent self-healing property, and satisfactory electrical conductivity. *Adv. Funct. Mater.* **28**, 1804416 (2018).

16. Q. Chen, L. Zhu, C. Zhao, Q. Wang, J. Zheng, A robust, one-pot synthesis of highly mechanical and recoverable double network hydrogels using thermoreversible sol-gel polysaccharide. *Adv. Mater.* **25**, 4171–4176 (2013).

17. S. Y. Zheng, H. Ding, J. Qian, J. Yin, Z. L. Wu, Y. Song, Q. Zheng, Metal-coordination complexes mediated physical hydrogels with high toughness, stick–slip tearing behavior, and good processability. *Macromolecules* **49**, 9637–9646 (2016).

18. P. Lin, S. Ma, X. Wang, F. Zhou, Molecularly engineered dual-crosslinked hydrogel with ultrahigh mechanical strength, toughness, and good self-recovery. *Adv. Mater.* **27**, 2054–2059 (2015).

19. Y. Yang, X. Wang, F. Yang, H. Shen, D. Wu, A universal soaking strategy to convert composite hydrogels into extremely tough and rapidly recoverable double-network hydrogels. *Adv. Mater.* **28**, 7178–7184 (2016).

20. J. Li, Z. Suo, J. J. Vlassak, Stiff, strong, and tough hydrogels with good chemical stability. *J. Mater. Chem. B* **2**, 6708–6713 (2014).

21. R. Long, K. Mayumi, C. Creton, T. Narita, C.-Y. Hui, Time dependent behavior of a dual cross-link self-healing gel: Theory and experiments. *Macromolecules* **47**, 7243–7250 (2014).

22. S. C. Grindy, R. Learsch, D. Mozhdehi, J. Cheng, D. G. Barrett, Z. Guan, P. B. Messersmith, N. Holten-Andersen, Control of hierarchical polymer mechanics with bioinspired metal-coordination dynamics. *Nat. Mater.* **14**, 1210–1216 (2015).

23. J. Fang, A. Mehlich, N. Koga, J. Huang, R. Koga, X. Gao, C. Hu, C. Jin, M. Rief, J. Kast, D. Baker, H. Li, Forced protein unfolding leads to highly elastic and tough protein hydrogels. *Nat. Commun.* **4**, 2974 (2013).

24. E. A. Appel, R. A. Forster, A. Koutsioubas, C. Toprakcioglu, O. A. Scherman, Activation energies control the macroscopic properties of physically cross-linked materials. *Angew. Chem. Int. Ed.* **53**, 10038–10043 (2014).

25. D. E. Fullenkamp, L. He, D. G. Barrett, W. R. Burghardt, P. B. Messersmith, Mussel-inspired histidine-based transient network metal coordination hydrogels. *Macromolecules* **46**, 1167–1174 (2013).

26. M. J. Harrington, A. Masic, N. Holten-Andersen, J. H. Waite, P. Fratzl, Iron-clad fibers: A metal-based biological strategy for hard flexible coatings. *Science* **328**, 216–220 (2010).

27. B. P. Lee, P. B. Messersmith, J. N. Israelachvili, J. H. Waite, Mussel-inspired adhesives and coatings. *Annu. Rev. Mater. Res.* **41**, 99–132 (2011).

28. W. T. Morgan, The histidine-rich glycoprotein of serum has a domain rich in histidine, proline, and glycine that binds heme and metals. *Biochemistry* **24**, 1496–1501 (1985).

29. A. Jancsó, A. Kolozsi, B. Gyurcsik, N. V. Nagy, T. Gajda, Probing the Cu^{2+} and Zn^{2+} binding affinity of histidine-rich glycoprotein. *J. Inorg. Biochem.* **103**, 1634–1643 (2009).

30. W. Ott, M. A. Jobst, M. S. Bauer, E. Durner, L. F. Milles, M. A. Nash, H. E. Gaub, Elastin-like polypeptide linkers for single-molecule force spectroscopy. *ACS Nano* **11**, 6346–6354 (2017).

31. G. I. Bell, Models for the specific adhesion of cells to cells. *Science* **200**, 618–627 (1978).

32. E. Evans, K. Ritchie, Strength of a weak bond connecting flexible polymer chains. *Biophys. J.* **76**, 2439–2447 (1999).

33. Y. Sun, W. Di, Y. Li, W. Huang, X. Wang, M. Qin, W. Wang, Y. Cao, Mg^{2+}-Dependent high mechanical anisotropy of three-way-junction pRNA as revealed by single-molecule force spectroscopy. *Angew. Chem. Int. Ed. Engl.* **56**, 9376–9380 (2017).

34. L. R. G. Treloar, *The Physics of Rubber Elasticity* (Oxford Univ. Press, New York, 1975).

35. J. Liu, C. S. Y. Tan, Z. Yu, Y. Lan, C. Abell, O. A. Scherman, Biomimetic supramolecular polymer networks exhibiting both toughness and self-recovery. *Adv. Mater.* **29**, 1604951 (2017).

36. J. A. Stella, A. D'Amore, W. R. Wagner, M. S. Sacks, On the biomechanical function of scaffolds for engineering load-bearing soft tissues. *Acta Biomater.* **6**, 2365–2381 (2010).

37. M. Enke, S. Bode, J. Vitz, F. H. Schacher, M. J. Harrington, M. D. Hager, U. S. Schubert, Self-healing response in supramolecular polymers based on reversible zinc–Histidine interactions. *Polymer* **69**, 274–282 (2015).

38. X. Yi, J. He, X. Wang, Y. Zhang, G. Tan, Z. Zhou, J. Chen, D. Chen, R. Wang, W. Tian, P. Yu, L. Zhou, C. Ning, Tunable mechanical, antibacterial, and cytocompatible hydrogels based on a functionalized dual network of metal coordination bonds and covalent crosslinking. *ACS Appl. Mater. Interfaces* **10**, 6190–6198 (2018).

39. N. B. Tito, C. Creton, C. Storm, W. G. Ellenbroek, Harnessing entropy to enhance toughness in reversibly crosslinked polymer networks. *Soft Matter* **15**, 2190–2203 (2019).

40. K. Mayumi, J. Guo, T. Narita, C. Y. Hui, C. Creton, Fracture of dual crosslink gels with permanent and transient crosslinks. *Ex. Mechan. Lett.* **6**, 52–59 (2016).

41. S. Zechel, M. D. Hager, T. Priemel, M. J. Harrington, Healing through histidine: Bioinspired pathways to self-healing polymers via imidazole–metal coordination. *Biomimetics* **4**, 20 (2019).

42. J. Wątły, A. Hecel, M. Rowińska-Żyrek, H. Kozłowski, Impact of histidine spacing on modified polyhistidine tag – Metal ion interactions. *Inorg. Chim. Acta* **472**, 119–126 (2018).

43. D. J. Huey, J. C. Hu, K. A. Athanasiou, Unlike bone, cartilage regeneration remains elusive. *Science* **338**, 917–921 (2012).

44. N. Kitamura, M. Yokota, T. Kurokawa, J. P. Gong, K. Yasuda, In vivo cartilage regeneration induced by a double-network hydrogel: Evaluation of a novel therapeutic strategy for femoral articular cartilage defects in a sheep model. *J. Biomed. Mater. Res. A* **104**, 2159–2165 (2016).

45. S. Azevedo, A. M. S. Costa, A. Andersen, I. S. Choi, H. Birkedal, J. F. Mano, Bioinspired ultratough hydrogel with fast recovery, self-healing, injectability and cytocompatibility. *Adv. Mater.* **29**, 1700759 (2017).

46. V. X. Truong, M. P. Ablett, S. M. Richardson, J. A. Hoyland, A. P. Dove, Simultaneous orthogonal dual-click approach to tough, in-situ-forming hydrogels for cell encapsulation. *J. Am. Chem. Soc.* **137**, 1618–1622 (2015).

47. S. Lin, Y. Zhou, X. Zhao, Designing extremely resilient and tough hydrogels via delayed dissipation. *Ex. Mechan. Lett.* **1**, 70–75 (2014).

48. J. Li, A. D. Celiz, J. Yang, Q. Yang, I. Wamala, W. Whyte, B. R. Seo, N. V. Vasilyev, J. J. Vlassak, Z. Suo, D. J. Mooney, Tough adhesives for diverse wet surfaces. *Science* **357**, 378–381 (2017).

49. S. J. Lau, B. Sarkar, Ternary coordination complex between human serum albumin, copper (II), and L-histidine. *J. Biol. Chem.* **246**, 5938–5943 (1971).

50. Z. Movasaghi, S. Rehman, I. U. Rehman, Raman spectroscopy of biological tissues. *Appl. Spectrosc. Rev.* **42**, 493–541 (2007).

51. C. N. Z. Schmitt, Y. Politi, A. Reinecke, M. J. Harrington, Role of sacrificial protein–metal bond exchange in mussel byssal thread self-healing. *Biomacromolecules* **16**, 2852–2861 (2015).

52. M. C. Boyce, E. M. Arruda, Constitutive models of rubber elasticity: A review. *Rubber Chem. Technol.* **73**, 504–523 (2000).

53. S. Cai, Z. Suo, Mechanics and chemical thermodynamics of phase transition in temperature-sensitive hydrogels. *J. Mech. Phys. Solids* **59**, 2259–2278 (2011).

54. Q. Fan, B. Chen, Y. Cao, Constitutive model reveals the defect-dependent viscoelasticity of protein hydrogels. *J. Mech. Phys. Solids* **125**, 653–665 (2019).

55. J. F. Marko, E. D. Siggia, Stretching DNA. *Macromolecules* **28**, 8759–8770 (1995).

56. A. Dong, J. Matsuura, S. D. Allison, E. Chrisman, M. C. Manning, J. F. Carpenter, Infrared and circular dichroism spectroscopic characterization of structural differences between β-lactoglobulin A and B. *Biochemistry* **35**, 1450–1457 (1996).

57. H. Jia, Z. Huang, Z. Fei, P. J. Dyson, Z. Zheng, X. Wang, Unconventional tough double-network hydrogels with rapid mechanical recovery, self-healing, and self-gluing properties. *ACS Appl. Mater. Inter.* **8**, 31339–31347 (2016).